Dipole−Dipole Electronic Energy Transfer: Fluorescence Decay Functions for Arbitrary Distributions of Donors and Acceptors in Systems with Cylindrical Symmetry

J. P. S. Farinha,*,† John G. Spiro,‡ and M. A. Winnik*,‡

Centro de Química-Física Molecular, Instituto Superior Técnico, 1049-001 Lisboa, Portugal, and Department of Chemistry, University of Toronto, 80 St. George Street, Toronto, Ontario, Canada M5S 3H6

Received: May 4, 2004; In Final Form: July 16, 2004

We extended our earlier models for direct resonance energy transfer (DET) on systems of planar and spherical symmetry to cylindrical domains. The model we now develop applies to systems with restricted geometries and arbitrary distribution functions of donors and acceptors with cylindrical symmetry. The method enables one to evaluate the donor decay function from the donor and acceptor concentration profiles without requiring prior calculation of the donor−acceptor pair distribution, even when the donor translational invariance requirements of the Klafter−Blumen methodology are not satisfied. The formalism was applied to simple systems in which the donors may or may not occupy equivalent positions. For the first case, our results are compared to and are shown to agree with previously known models. For the second case, we have obtained new expressions for the donor decay function. Finally, we discuss whether certain specific geometries could be distinguished from one another by single-photon-timing fluorescence measurements on dye-labeled samples.

Introduction

Nanotechnology, the ability to synthesize, manipulate, and characterize structures involving polymers and other materials that form domains with at least one dimension on the nanometer scale, is attracting a great deal of interest for its current and expected applications in photonics, data storage, catalysis, separation processes, nanosensors, biotechnology, and other fields. Many small particles of cylindrical symmetry and high axial ratio, such as nanotubes and nanowires, have been prepared.

Among synthetic tools, the molecular self-assembly of block copolymers has attracted a great deal of interest.[1] Until recently, research on the morphology of block copolymers focused primarily on the bulk properties of melts; the periodic lamellar structures that are formed when the components of a diblock copolymer are approximately of the same volume[2−4] have been particularly thoroughly studied because of their simple geometry and the relative ease with which equilibrium systems may be obtained.[5] However, over the past decade there has been increased interest in thin films and also in cylindrical block copolymer structures to be used as templates in connection with nanotechnology.[6]

Of the numerous and widely different approaches that can lead to cylindrical (and other) structures, we will mention only a few here: etching away one of the blocks,[7,8] cross-linking the core[9] or the shell (corona)[10] of cylindrical micelles, adjusting the properties of a block copolymer supramolecular assembly with a low-molar-mass additive,[6] and the use of block copolymers for structure directing in organically modified inorganic mesostructures.[11] It is thought[12] that industrial production of new structural materials based on nanotube composites is just a few years away.

Morphological and other information on nanostructures is frequently derived from the analysis of fluorescence and fluorescence decay data.[13,14] Here again, lamellar or spherical geometries were usually dealt with, but cylindrical or presumed cylindrical nanostructures have also been considered to be models, particularly for dyes adsorbed on silica.[15] In the polymer field, we are aware of two studies pertaining to the latter (i.e., cylindrical) types of systems.[16,17]

We have had longstanding involvement in direct nonradiative electronic energy transfer (DET) studies, which involve labeling the domain(s) of interest with appropriate donor and acceptor dye moieties. One measures and analyzes the fluorescence decay of the donors, $I_D(t)$, in the presence of varying concentrations of acceptors. Concentration profiles of the dyes, which in turn are dictated by the geometry and physics of the system, are inferred from such experiments (usually) through least-squares analysis of the data using appropriate mathematical models.[18]

In DET experiments, one measures the increase in the rate of fluorescence decay from an inherent value of $1/\tau_D$, where τ_D is the donor (D) lifetime in the absence of acceptors (A), to a rate of $w + 1/\tau_D$ in the presence of A. The measured rate of DET is then related to the distance r separating the centers of the transition dipoles of D and A via Förster's relation[19]

$$w(r) = \frac{3\kappa^2}{2\tau_D}\left(\frac{R_0}{r}\right)^6 \qquad (1)$$

In eq 1, the factor of $3\kappa^2/2$ is determined by the orientation of the transition moments of the excited donor (D*) and A, and R_0 is a constant (Förster radius) that can be calculated from the photophysical properties of the D/A pair[19] and normally has a value in the range of 2−7 nm.

Early treatments of DET kinetics considered systems with uniform D and A distributions over extended space in one to three dimensions. When the D and A groups are distributed in a system of restricted geometry, that is, over domains that are

* Corresponding authors. E-mail: farinha@ist.utl.pt; mwinnik@chem.utoronto.ca.
† Instituto Superior Técnico.
‡ University of Toronto. E-mail: jspiro@chem.utoronto.ca.

10.1021/jp0480807 CCC: $27.50
Published on Web 09/29/2004

finite in size with at least one dimension on the order of R_0, edge effects become important. Such effects were initially explored by Fayer and co-workers for D−D energy migration[20] and Klafter, Blumen, and co-workers for energy transfer (D−A DET).[15,21,22] In the Klafter−Blumen formulation, the DET-related survival probability of an excited donor at position $\vec{r}_0$ and as a function of time t is given by

$$\phi(t, \vec{r}_0) = \exp\{-p\int_V [1 - \exp(-w(r)t)]\rho(r)\, dV\} \quad (2)$$

where p is the probability that an allowed acceptor site is actually occupied (which is proportional to the overall bulk A concentration); $w(r)$ is the rate of DET given by eq 1; $\rho(r)$ is the distribution function for the separation distance of D−A pairs; and the integration is carried out over the volume V of the microdomain under consideration.

Unfortunately, eq 2 applies only in situations where all donors are in equivalent environments (i.e., when each donor "sees" the same distribution of acceptors around itself). Even then, obtaining the site density function $\rho(r)$ may be difficult.[23] Because of the foregoing difficulties, various simplifying assumptions are usually introduced regarding the distribution of dyes and hence regarding the nanostructure involved. However, we and our associates have published a number of papers[24−27] that allow fluorescence decay analyses and simulations for very general donor and acceptor distributions over domains of restricted geometry, provided one can assume planar or spherical symmetry for the systems.

To our knowledge, DET algorithms for cylindrical systems have not been elaborated to the level of generality in the preceding references.[24−27] Rather, one of three simplifying assumptions has always been used: (i) all dyes are located on the surface of a cylinder;[21] (ii) donors are on the surface and acceptors inside the (same) cylinder;[22] or (iii) donors are located on the axis of the cylinder, with acceptors on the surface and inside.[22] In these cases, all donor dyes are in equivalent positions; that is, each of them is surrounded by an exactly equal distribution of acceptors. Furthermore, in all of these models it has also been assumed that, apart from the specific restrictions mentioned, the dyes are homogeneously distributed in their domains.

Here, we present equations/algorithms for systems of cylindrical symmetry where the donor dyes lack translational invariance and are at the same level of generality as those that we earlier proposed for planar and spherical geometries.[24−27] In principle, the method is straightforward, and we will illustrate its power by discussing its application to a specific system, represented by a more general model than those previously available.[15,21,22] In a companion paper,[28] we will discuss a more complex application, namely, whether it may be possible to determine the thickness of circular interfaces[29] in hexagonal Wigner−Seitz cells of AB diblock copolymer melts[30,31] by fluorescence decay measurements on dye-labeled samples.

Model

Our line of development is somewhat different here than in our earlier reports on planar and spherical systems[24−27] because the intersections of spherical shells, representing acceptors at fixed distances from a given donor, with cylinders that are the natural objects for specifying dye concentrations in this geometry, are given by complex equations involving elliptic integrals.[32] To avoid this problem, our starting point will be an equation similar to eq 11 of reference 26; that is, we will consider the number of acceptors in appropriate volume elements and their distance from representative donors.

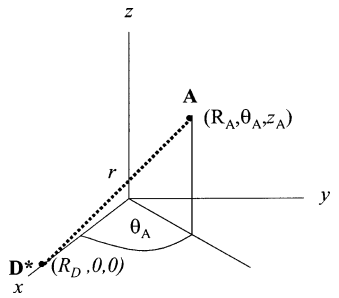

Figure 1. Energy transfer from an excited donor at a distance R_D from the axis of the cylindrical structure to an acceptor at a distance R_A from the axis.

Because of the cylindrical symmetry, it will be convenient to consider first donors located on the surface of a specific cylinder of radius R_D and acceptors located on a concentric cylindrical shell of radius R_A and thickness dR_A. We "count up" the number of acceptors located in a volume element $R_A\, dR_A\, d\theta_A\, dz_A$ at the cylindrical coordinates (R_A, θ_A, z_A) and note that their distance from a donor at $\vec{r}_D = (R_D, 0, 0)$ is (Figure 1)

$$r = (R_D^2 + R_A^2 + z_A^2 - 2R_A R_D \cos\theta_A)^{1/2} \quad (3)$$

The energy-transfer probability $\phi(t, R_D)$ for the donor located at (R_D, 0, 0) will then be given by

$$-\frac{\ln[\phi(t, R_D)]}{4} = \int_0^\infty dz_A \int_0^\infty R_A C_A(R_A)\, dR_A \int_0^\pi \{1 - \exp[-w(r)t]\}\, d\theta_A \quad (4)$$

where $C_A(R_A)$ is the acceptor number density (number of acceptors per nm^3) at the cylinder whose radius is R_A and $w(r)$ is obtained by substituting eq 3 into eq 1.

If we now consider a cylindrical object of total length L, then the donor decay law including the intrinsic deactivation of the donor with lifetime τ_D is obtained by integration over all possible donor positions

$$I_D(t) = \exp\left(-\frac{t}{\tau_D}\right)\int_0^{L/2} 2dz_D \int_0^{2\pi} d\theta_D \int_0^\infty R_D C_D(R_D)\, \phi(t, R_D)\, dR_D \quad (5)$$

which simplifies to

$$I_D(t) = 2\pi L \exp\left(-\frac{t}{\tau_D}\right)\int_0^\infty R_D C_D(R_D)\, \phi(t, R_D)\, dR_D \quad (6)$$

with $\phi(t, R_D)$ given by eq 4 and $C_D(R_D)$ the donor concentration profile. Using eqs 3, 4, and 6, we can calculate the donor fluorescence decay profile for virtually any distribution of donors and acceptors obeying cylindrical symmetry. The expressions are exact. The only assumption involved pertains to the orientation factor, which we preaverage either in the dynamic or the static regimes.[33] We note that $C_A(R_A)$ must have units expressed as number density, but $C_D(R_D)$ can have any unit of concentration because $I_D(t)$ is normalized when compared with experimental measurements.

In eqs 4 and 6, we have set the limits of integration from zero to infinity for the convenience of dealing with continuously extended concentration profiles. However, for systems with restricted geometry or finite size, $C_A(R_A)$ and $C_D(R_D)$ can be

associated with appropriate truncating functions that will restrict the domain of integration. In the examples to follow, we make use of truncation to restrict this integration limit. The lower limit of integration $R_A = 0$ in eq 4 implicitly allows for the possibility of donors and acceptors occupying the same position in space. This way we gain analytical simplicity, but we also introduce an error that can affect the very early fluorescence decay times. This error is sometimes ignored because it has a low impact on analyzing experimental fluorescence decay data because the rate of DET between very close pairs is extremely high. Donors in close proximity to acceptors do not contribute significantly to the detected emission. However, to keep our formalism as general as possible, we will remove this assumption by establishing a minimum donor−acceptor encounter distance R_e. This is usually taken to be the sum of the donor and acceptor van der Waals radii.[34] In the algorithms, we could just exclude all values $r < R_e$ (with r given by eq 3) when integrating eq 4 numerically. Although this method may become appropriate in future calculations, here we will employ equations that will be more convenient for specific, simple systems. We therefore define a cylindrical analogue of the donor−acceptor encounter limitation proposed by Levitz, Drake, and Klafter in their lattice model.[21] The exclusion cylinder will have a radius R_e and height $2R_e$, centered on the donor located at $\vec{r}_D$. Consistent with this lattice concept, we will not attempt to compute explicitly the extent of quenching for donor sites closer than R_e from the axis of the cylinder but will only extrapolate into that region. (However, R_e can be arbitrarily small.)

For a cylindrical system of infinite length (the usual approximation),[21,22] the local survival probability of our representative donor at $\vec{r}_D$ will now be given by a volume integral, which may be expressed as sums of iterated integrals. (To do so, we must show that the integrand obeys uniform convergence requirements,[35] but this has always been the case for the particular systems that we have considered.)

$$
\begin{aligned}
-\frac{\ln[\phi(t,\vec{r}_D)]}{4} = {} & \int_{R_e}^{\infty} dz_A \int_{R_D-R_e}^{R_D+R_e} R_A C_A(R_A)\, dR_A \int_0^{\alpha} \times \\
& \{1-\exp[-w(r)t]\}\, d\theta_A + \\
& \int_0^{\infty} dz_A \{ \int_0^{R_D-R_e} R_A C_A(R_A)\, dR_A \int_0^{\pi} \times \\
& \{1-\exp[-w(r)t]\}\, d\theta_A + \\
& \int_{R_D+R_e}^{\infty} R_A C_A(R_A)\, dR_A \int_0^{\pi} \times \\
& \{1-\exp[-w(r)t]\}\, d\theta_A + \\
& \int_{R_D-R_e}^{R_D+R_e} R_A C_A(R_A)\, dR_A \int_{\alpha}^{\pi} \times \\
& \{1-\exp[-w(r)t]\}\, d\theta_A\}
\end{aligned}
\tag{7}
$$

where α is the angle between $\vec{r}_D$ and $\vec{r}_A$ vectors projected into the $z = 0$ plane and at a distance R_e apart there (i.e., $\cos\alpha = \{(R_D^2 + R_A^2 - R_e^2)\}/\{(2R_AR_D)\}$).

It may be appropriate to elaborate somewhat on the terms of eq 7. Readers will note that the inner double integral of the first term references the acceptor "exclusion" region in the $z = 0$ plane: $\{(R_A, \theta_A)|(R_D^2 + R_A^2 - 2R_AR_D\cos\theta_A)^{1/2} < R_e\}$. The second improper integral counts up acceptors outside the exclusion region and computes the quenching due to them. In some cases, it will be advantageous to rearrange eq 7 (again, subject to uniform convergence requirements):

$$
\begin{aligned}
-\frac{\ln[\phi(t,\vec{r}_D)]}{4} = {} & \int_{R_e}^{\infty} dz_A \int_0^{\infty} R_A C_A(R_A)\, dR_A \int_0^{\pi} \times \\
& \{1-\exp[-w(r)t]\}\, d\theta_A + \\
& \int_0^{R_e} dz_A \{ \int_0^{R_D-R_e} R_A C_A(R_A)\, dR_A \int_0^{\pi} \times \\
& \{1-\exp[-w(r)t]\}\, d\theta_A + \\
& \int_{R_D+R_e}^{\infty} R_A C_A(R_A)\, dR_A \int_0^{\pi} \times \\
& \{1-\exp[-w(r)t]\}\, d\theta_A + \\
& \int_{R_D-R_e}^{R_D+R_e} R_A C_A(R_A)\, dR_A \int_{\alpha}^{\pi} \times \\
& \{1-\exp[-w(r)t]\}\, d\theta_A\}
\end{aligned}
\tag{8}
$$

The donor survival probability for our cylindrical system is obtained by averaging over all cylinders of radius R_D:

$$
I_D(t) = \exp\left(-\frac{t}{\tau_D}\right) \int_V C_D(R_D)\, \phi(t,\vec{r}_D)\, dV \tag{9}
$$

where $dV = R_D\, dR_D\, d\theta_D\, dz_D$. Subsequent normalization leads to the measurable donor fluorescence intensity for specific systems.

In real nanostructures involving polymers and other materials that form domains with at least one dimension on the nanometer scale, one deals with distribution profiles that most likely are spatially extended and nonuniform. Here, we consider simple systems consisting of uniform and sharply discontinuous concentration profiles. The extension to systems without sharp boundaries, where donors and acceptors have nonhomogeneous concentration profiles, is straightforward as long as one has a pertinent physical theory to describe the concentration profiles. As mentioned earlier, in a companion paper[28] we will discuss such an application dealing with cylindrical block copolymer interfaces. (Fluorescence techniques could become important there because of the scarcity of data available.)

Before demonstrating how the new model can be used to analyze fluorescence decay data, we wish to show that it is consistent with earlier published, simpler models for cylindrical systems (Figure 2a−c).[21,22] In the latter cases, all donors have equivalent loci within the restricted space of a cylinder of radius R (i.e., each donor is surrounded by the same uniform distribution of acceptors). Next, we will consider a system (Figure 2d) where the donor positions are *not* equivalent. To our knowledge, there is no published analysis of such systems.

a. Donors on the Axis, Acceptors Uniformly Distributed inside a Cylinder. The model geometry is a cylinder of radius R and infinite length (Figure 2a), where the donors are uniformly distributed along the axis of the cylinder and the acceptors fill the inside of it. In terms of the general equations (eqs 7 and 8), we are dealing with a Dirac delta function for the donor concentration ($R_DC_D(R_D) = C_D^0\, \delta(R_D)$, where C_D^0 is the average donor concentration over the axis of the cylinder) and a Heaviside function for the acceptor concentration profile ($C_A(R_A) = C_A^0\, H(R - R_A)$, with $H(x) = 1$ for $x > 0$ and $H(x) = 0$ for $x \le 0$; where C_A^0 is the bulk-average acceptor concentration). Because our model assumes $R_e \le R_D$, in this case we must have $R_e = 0$. Equations 7 (or 8) and 9 then simplify to

$$
I_D(t) = \exp\left(-\frac{t}{\tau_D}\right) \phi(t,(0,0,0)) \tag{10}
$$

$$\phi(0,0,0) = \exp\{-4\pi C_A^0 \int_0^\infty dz_A \int_0^R R_A \times \{1 - \exp[-w[(R_A^2 + z_A^2)^{1/2}]t]\}\, dR_A\} \quad (11)$$

(i.e., we obtain the published equation,[22] which can be derived from eq 2 without resorting to our more general methods).

b. Donors and Acceptors Uniformly Distributed on the Surface of a Cylinder. The case where donors and acceptors are both randomly distributed on the surface of an infinite cylinder of radius R (Figure 2b) was treated by Levitz, Drake, and Klafter.[21] In our notation, their equation may be written as

$$I_D(t) = \exp\left(-\frac{t}{\tau_D}\right)\exp\left(-\frac{4p}{s^2}\left\{\int_s^\infty dz \int_0^{2R} \frac{dr}{[1 - r^2/(4R^2)]^{1/2}}\left[1 - \exp\left(-\frac{3\kappa^2 R_0^6 t}{2\tau_D(z^2 + r^2)^3}\right)\right] + \int_0^s dz \int_s^{2R} \frac{dr}{[1 - r^2/(4R^2)]^{1/2}}\left[1 - \exp\left(-\frac{3\kappa^2 R_0^6 t}{2\tau_D(z^2 + r^2)^3}\right)\right]\right\}\right) \quad (12)$$

where s is the average size of donor and acceptor molecules and p is the fraction of surface sites occupied by acceptors. Here, both the donor and acceptor concentration profiles are described by Dirac delta functions in eqs 7 and 9 ($C_D(R_D) = C_D^0\, \delta(R_D - R)$, $C_A(R_A) = C_A^0\, \delta(R_A - R)$), and readers will note that the average acceptor concentration, C_A^0, is equivalent to Levitz, Drake, and Klafter's p/s^2 prefactor with $s = R_e$. In this case, eq 8 immediately simplifies to

$$-\frac{\ln\{\phi[t, (R, 0, 0)]\}}{4} = C_A^0 R \int_{R_e}^\infty dz_A \int_0^\pi \times \left\{1 - \exp\left[-\frac{3\kappa^2 R_0^6 t}{2\tau_D[2R^2(1 - \cos\theta_A) + z_A^2]^3}\right]\right\} d\theta_A + C_A^0 R \int_0^{R_e} dz_A \int_{\cos^{-1}\left(1 - \frac{R_e^2}{2R^2}\right)}^\pi \times \left\{1 - \exp\left[-\frac{3\kappa^2 R_0^6 t}{2\tau_D[2R^2(1 - \cos\theta_A) + z_A^2]^3}\right]\right\} d\theta_A \quad (13)$$

The substitution $2R^2(1 - \cos\theta_A) = r^2$ and the above-mentioned equivalences now lead to eq 12.

c. Donors Uniformly Distributed on the Surface, Acceptors inside a Cylinder. We will now show that Blumen, Klafter, and Zumofen's[22] local survival probability expression (BKZ model) for donors randomly distributed on the surface and acceptors inside an infinite cylinder of radius R (Figure 2c)

$$-\frac{\ln[\phi(t)]}{4} = C_A^0 \int_0^{2R} dr \int_0^\infty dz\, r \cos^{-1} \times \left(\frac{r}{2R}\right)\left[1 - \exp\left(-\frac{3\kappa^2 R_0^6 t}{2\tau_D(z^2 + r^2)^3}\right)\right] \quad (14)$$

can also be obtained from our model, eqs 7 and 8. First, we note that the differential $dz\, r \cos^{-1}(r/2R)\, dr$ counts up the number of acceptors in a dz-thick slice of the cylinder along a circular shell of thickness dr inscribed in the slice in such a manner that each acceptor is at a distance r from the reference donor. Double integration over $[0, \infty) \times [0, 2R]$ then accounts for all

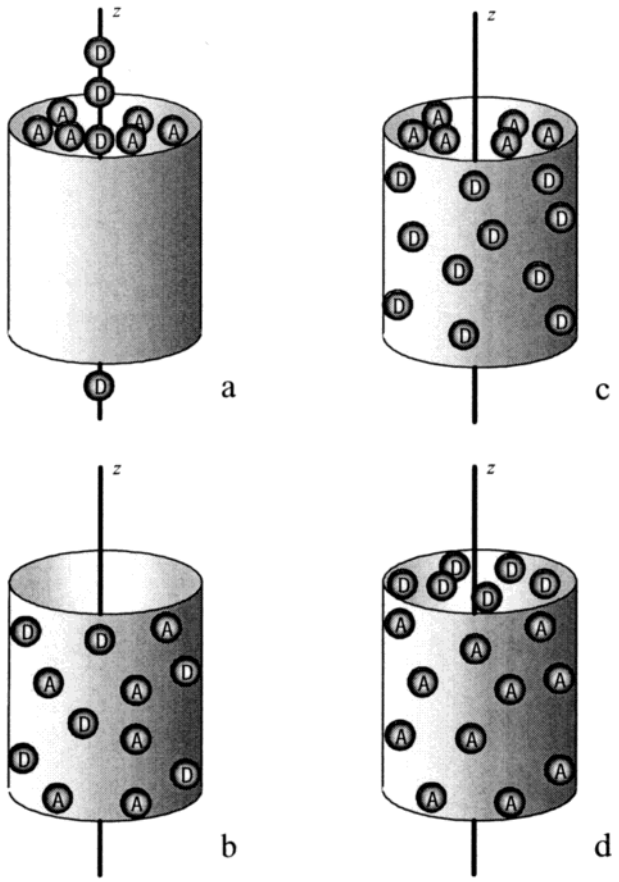

Figure 2. Random but isotropic distributions of donors (D) and acceptors (A) in a cylinder of radius R and infinite length: (a) D on the axis and A inside; (b) D and A on the surface; (c) D on the surface and A inside; (d) D inside and A on the surface. In cases a−c, all donors occupy translationally invariant positions. In d, donors "see" different acceptor distributions depending on their position inside the cylinder.

of the acceptors in the cylinder. The BKZ model does not exclude acceptors in the immediate neighborhood of the reference donor ($R_e \to 0$). In the limit of $R_e \to 0$, for $C_D(R_D) = C_D^0\, \delta(R_D - R)$ and $C_A(R_A) = C_A^0 H(R - R_A)$, eqs 7 and 8 become

$$-\frac{\ln[\phi(t, \vec{r}_D)]}{4} = \int_0^\infty dz_A \int_0^R R_A C_A^0\, dR_A \int_0^\pi \times \left\{1 - \exp\left[-\frac{3\kappa^2 R_0^6 t}{2\tau_D(R^2 + R_A^2 + z_A^2 - 2RR_A\cos\theta_A)^3}\right]\right\} d\theta_A \quad (15)$$

Again, one is counting up acceptors at a distance $r = (R^2 + R_A^2 + z_A^2 - 2RR_A\cos\theta)^{1/2}$ from a reference donor (on the surface of the cylinder), only the enumeration scheme is different: one counts along dz_A-thick slices of cylindrical shells of thickness dR_A. The triple integral still covers all of the acceptors in (one-quarter of) the cylinder.

Some readers may not be entirely convinced by the foregoing geometric argument. In the Appendix, we show that for short decay times, where the expansion of the exponential functions in eqs 14 and 15 can be truncated after the linear term, and for a representative cylinder diameter of 10 nm, numerical evaluation of the multiple integrals of eqs 14 and 15 yields identical results (to eight significant figures).

d. Donors Inside, Acceptors Uniformly Distributed on the Surface of a Cylinder. This is a system where the donors lack translational invariance, a situation that the Klafter−Blumen formalism (eq 2) cannot accommodate. Again, we consider a cylinder of radius R and infinite length (Figure 2d).

Similarly to the BKZ morphology[22] discussed in subsection c (but with D and A in reversed positions), we now have to evaluate eqs 7−9 with a Dirac delta function for the acceptor concentration, $C_A(R_A) = C_A^0\,\delta(R_A - R)$, and a step function for the donor concentration profile, $C_D(R_D) = C_D^0\,H(R - R_D)$. (However, as mentioned earlier, we will restrict R_D to values no smaller than R_e; we will only extrapolate into the $R_D < R_e$ region.) Again, C_D^0 and C_A^0 are the average dye concentrations for the whole cylinder and its surface, respectively. Equation 7 (or 8) now leads to the local survival probability expressions

$$-\frac{\ln[\phi(t, \vec{r}_D)]}{4} = RC_A^0\int_0^\infty dz_A \int_0^\pi \{1 - \exp[-w(r)t]\}\, d\theta_A \tag{16a}$$

for $R_e < R_D < R - R_e$ (we assume $R > 2R_e$) and

$$-\frac{\ln[\phi(t, \vec{r}_D)]}{4} = RC_A^0\int_{R_e}^\infty dz_A \int_0^\pi \{1 - \exp[-w(r)t]\}\, d\theta_A + RC_A^0\int_0^{R_e} dz_A \int_\alpha^\pi \{1 - \exp[-w(r)t]\}\, d\theta_A \tag{16b}$$

for $R - R_e \le R_D < R$, with $\alpha = \cos^{-1}\dfrac{R_D^2 + R^2 - R_e^2}{2RR_D}$.

Here, $w(r)$ is obtained from eqs 1 and 3 as

$$w(r) = \frac{3\kappa^2 R_0^6}{2\tau_D(R^2 + R_D^2 + z_A^2 - 2RR_D\cos\theta_A)^3} \tag{16c}$$

Structure Identification

We are interested in the possibility of using DET to differentiate between cylindrical and spherical structures containing donors homogeneously distributed inside and acceptors on the surface. We will compare fluorescence decay curves computed[27] for two geometries with the same surface-to-volume ratio: 5.0-nm-radius cylinder and 7.5-nm-radius sphere. We will also consider a sphere with the same radius as the 5.0-nm-radius infinite cylinder.[49] It will be interesting to examine whether donor fluorescence decay ($I_D(t)$) measurements may be able to discriminate between the two geometries of equal surface-to-volume ratio and also between structures with the same radius because in some situations it would be useful to employ fluorescence methods to distinguish between (hexagonally stacked) cylinders and spheres of equal radius (previously determined by microscopy or small-angle scattering measurements). This knowledge will be particularly useful as a basis to extend our model to a situation where the surface of the nanocylinder is replaced by an interface of finite size. Then, the information obtained from imaging or scattering techniques on the nanostructure size and morphology would be complemented by the information given by DET on its interface thickness.[36]

We will present results here for an acceptor number density of 0.04 nm^{-2}. For the lattice-type model we are employing and for the 0.5-nm encounter radius, this corresponds to a probability of 0.01 that any given potential acceptor site is actually occupied. At higher acceptor concentration, potential "double occupation" of sites would be a concern; at lower concentrations, the extent of quenching would be harder to measure experimentally. Other parameters that we have assumed in our simulations are $R_0 = 2.3$ nm,[37] a dipole orientation factor $\langle\kappa^2\rangle$ of $^2/_3$ (rapidly reorienting dipoles, cf. eq 1), and an unquenched donor lifetime of 45.0 ns (typical in our experiments with phenanthrene and anthracene moieties as donors and acceptors). In earlier studies,[36] we found that computed fluorescence decays were not sensitive to the exact magnitude of R_e; 0.5 nm will be our choice in this report.

Before discussing the more rigorous computations utilizing eqs 9 and 16, we will present preliminary fluorescence quenching calculations according to Perrin's "active sphere" model.[38] This is an all-or-nothing static quenching model that assumes that if there is an acceptor within a distance R_p (we will use $R_p = R_0 = 2.3$ nm) of a donor, the D fluorescence will be quenched instantaneously; if not, there will be no quenching. Although it constitutes a crude approximation of the DET phenomenon, this model can be convenient to use in many situations, but to our knowledge, it has not been employed for the geometries dealt with in this section of our report.

To compute Perrin survival probabilities, we need to compute the area of that part of our cylindrical, or spherical, surface that is within a distance R_p from a donor located at (R_D, 0, 0) (in cylindrical or spherical coordinates, respectively). This is not a difficult task, using the theory of parametrized surfaces.[39] From the known acceptor concentration (in our case 0.04 nm^{-2}), we can calculate the survival probability of donors in a cylindrical or spherical shell centered on the radial distance R_D from the center of the cylinder or sphere. Averaging these survival probabilities, weighted by the volumes of the shells, gives the overall Perrin survival probability: 0.717 for the 5-nm-radius cylinder, 0.625 for the 5-nm-radius sphere, and 0.727 for the 7.5-nm-radius sphere. As was expected, there is considerably more quenching by acceptors in the more "compact" body (5-nm-radius sphere versus 5-nm-radius cylinder). However, there seems to be very little difference between cylinders and spheres of equal surface-to-volume ratio.

To answer the question of whether fluorescence decay measurements will be able to discriminate cylindrical and spherical morphologies of equal surface-to-volume ratio, we need to examine the results of the more precise computations: eqs 9 and 16 for cylinders and the methods of ref 27 for spheres. To allow for a finite (in our case $R_e = 0.5$ nm) encounter radius in inside-to-surface DET for spheres, the local survival probability equation (eq 24b of ref 27) had to be modified:

$$-\ln[\varphi(t, R_D)] = \frac{2\pi C_A R}{R_D}\int_{\max\{0.5,(R - R_D)\}}^{(R+R_D)} r\left[1 - \exp\left\{-\frac{t}{\tau_D}\left(\frac{R_0}{r}\right)^6\right\}\right] dr \tag{17}$$

The numerical integrations involved in evaluating eq 24a of ref 27 and eq 17 were quite straightforward, except that because of the greatly increased quenching near the surface of a sphere it was preferable to employ unequally spaced abscissas in the former. For the 5.0-nm-radius sphere, we chose the R_D values 0.0, 0.5, 1.0, 1.5, 1.8, ..., 3.9, 4.1, 4.3, 4.5, 4.6,..., 5.0 nm, and for the 7.5-nm-radius sphere, $R_D = 0.0$, 0.5,..., 4.0, 4.3,..., 6.1, 6.3, 6.5, 6.7, 6.8,..., 7.5 nm. The integration software was NAG routine D01GAF,[40] which uses finite-difference equations with error estimates, according to a method due to Gill and Miller.[41] (For eq 17, we used the adaptive routine NAG D01AJF.[40])

The integration tasks represented by eq 16 are more demanding than the computations for spheres. Fortunately, convenient

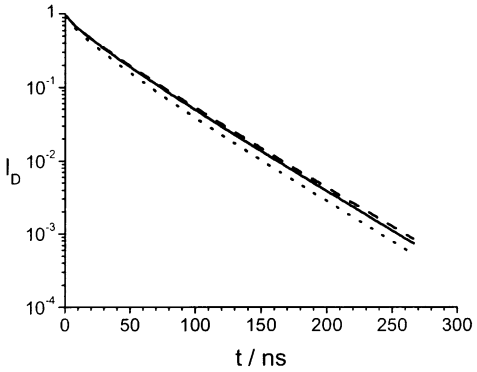

Figure 3. δ-function excitation fluorescence decay curves for the 5-nm-radius cylinder (−) and sphere (···) and for the 7.5-nm-radius sphere (- - -) donors inside/acceptors on the surface geometry. Acceptor concentration and photophysical parameters as discussed in the text.

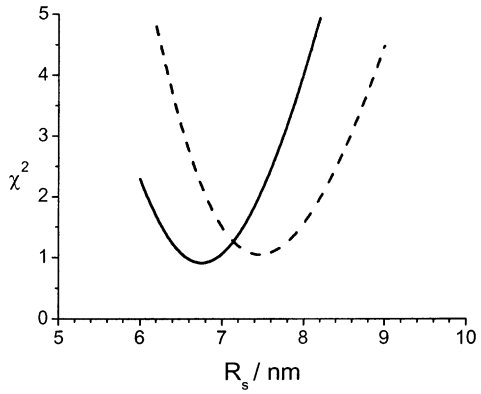

Figure 4. χ^2 values obtained from the analysis of experimental donor decay curves for donors inside/acceptors on the surface of a 5-nm-radius cylinder (−) and a 7.5-nm-radius sphere (- - -). Each curve corresponds to fitting a simulated experimental decay with donor survival probability functions simulated for different trial sphere radii.

double integration software was again available from NAG:[40] routine D01DAF. To evaluate the improper integrals of eqs 16a and b, we replaced the upper limits (∞) successively by 30, 60, and 120 nm, followed by Aitken extrapolations to infinity.[42]

In Figure 3, we present δ-function excitation decays for the three "donors inside/acceptors on the surface geometries" that we have already compared using our Perrin[38] models: 5-nm-radius cylinder, 5-nm-radius sphere, and 7.5-nm-radius sphere. Common parameters employed in the three computations are $\langle\kappa^2\rangle = {}^2/_3$, $\tau_D = 45.0$ ns, $R_0 = 2.3$ nm, $C_A = 0.04$ nm^{-2}, and $R_e = 0.5$ nm. Despite the approximate nature of the Perrin models, the conclusions obtained here are rather similar to the former results: decay rates are close to each other for different geometries with the same surface-to-volume ratio but much higher for the 5-nm-radius sphere than for the 5-nm-radius cylinder. Therefore, in principle, cylindrical and spherical structures of the same radius are easily distinguished by this method.

We will now examine whether one could distinguish between the different geometries with the same surface-to-volume ratio by analyzing experimental fluorescence decay curves obtained by the single-photon counting (SPC) technique. To do this, the noise-free simulated donor survival probability curves $I_D(t)$ obtained using the cylindrical and spherical models were convoluted with an experimental instrument response function $L(t)$ obtained from a real excitation source, as described previously:[43]

$$I_D^{conv}(t) = \int_0^t L(s)\, I_D(t-s)\, ds \qquad (18)$$

To the convoluted curves $I_D^{conv}(t)$, we then added Poisson noise to mimic experimental donor decays.[44,45] We refer to the simulated decays convoluted with real lamp excitation profiles and with added noise, I_D^{exptl}, as simulated experimental decays or just experimental decays for simplicity.

Direct analysis of these experimental decays using the new cylindrical model for DET would involve numerous local survival probability computations (eq 16) for various assumed values of the cylinder radius. One would have to evaluate double instead of single integrals, extrapolate to long cylinders, and assess the precision of the results. To avoid this, our strategy will be to analyze all experimental decays (simulated using the model for spheres or cylinders) by adjusting the model for DET in spheres[27] (eq 17).

First, we simulate donor survival probability curves using the spherical model of DET[27] for various trial particle radii (R_s), fixing all other parameters, which are usually known from calculation or from independent experiments. These simulated donor survival probability curves are then convoluted with the experimental instrument response function ($L(t)$) to obtain different trial donor decay profiles ($I_D^{spherical}(R_s, t)$). The latter are then compared with the experimental donor fluorescence decay profiles, allowing us to obtain an equivalent spherical radius.

Comparison of the experimental and spherical model trial decays is done by least squares

$$I_D^{exptl}(t) = a_N I_D^{spherical}(R_s, t) \qquad (19)$$

where the only fitting parameter is the normalization factor of the decay intensity, a_N. This is a weighted regression that takes into account the Poisson error of counting in the usual manner.[18] To evaluate the quality of the fitting results, we calculate the mean square error of the weighted regression, usually denoted by χ^2 in the single-photon timing literature, and plot the weighted residuals and autocorrelation of (weighted) residuals. Acceptable fitting results produce χ^2 close to 1, with randomly distributed weighted residuals and autocorrelation of residuals.

In Figure 4, we show the χ^2 values obtained for the analysis of decays for donors inside/acceptors on the surface of a 7.5-nm-radius sphere and a 5-nm-radius cylinder. The fitting results are good in both cases, with χ^2 for the best fitting value close to 1. For the 7.5-nm-radius sphere, we recover a sphere radius of 7.5 nm, as expected. However, the equivalent spherical radius obtained for the cylindrical geometry, $R_S = 6.7$ nm, is about 35% higher than the real cylinder radius ($R_C = 5$ nm).

Although the differences in the decay functions are very small for radii 0.5 nm higher or lower than the best fitting values, the corresponding autocorrelations of weighted residuals show fairly strong irregularities (Figure 5), allowing us to recover the radii with very good precision. The results suggest error bars of at most ± 0.5 nm (Figure 5a and b), with the recovered values of the radii being $R_S = 7.5 \pm 0.5$ nm for the sphere and $R_S = 6.7 \pm 0.5$ nm for the cylinder. Therefore, under the conditions chosen for our simulation the kinetics of DET for donors inside/acceptors on the surface of a cylinder and of a sphere of equal surface-to-volume ratio are too similar to be distinguished (i.e., the experimental cylindrical decay is well represented by the equations for DET in spherical geometry).

However, if the radius of the structure is known beforehand, one *can* distinguish between spherical and cylindrical geometries because the equivalent spherical radii obtained for the two cases

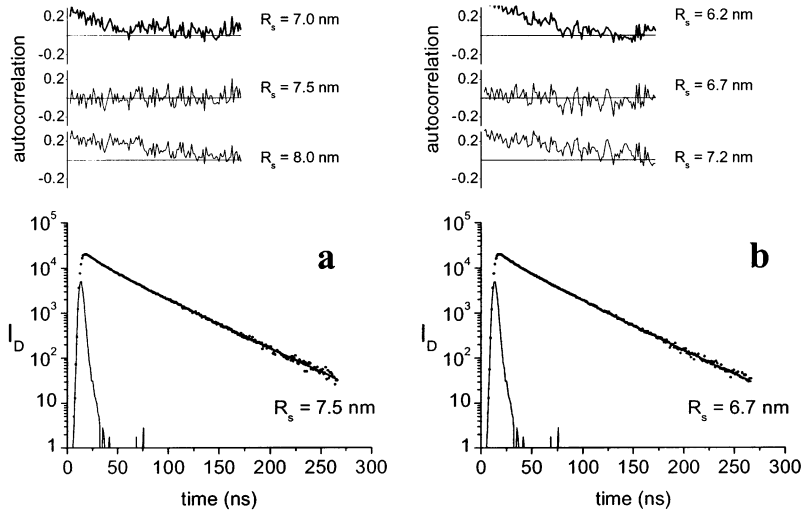

Figure 5. Experimental instrument response function and simulated experimental donor decay profiles obtained for a 7.5-nm-radius sphere (a) and a 5-nm-radius cylinder (b). Examination of the autocorrelation plots from trial fits allows a precision of better than 0.5 nm in recovering actual or equivalent spherical radii.

are sufficiently different. As pointed out by one of the reviewers, beyond the preceding theoretical considerations, in real life, experimental uncertainties would also hamper structure identification. For instance, donor aggregation may cause nonexponential decay even in the absence of acceptors. Nevertheless, the latter difficulty and some others can usually be resolved by improved synthetic or labeling procedures.

Conclusions

Extending earlier results[24−27] applicable to systems of planar or spherical symmetry, we have now obtained a theoretical expression (eqs 7−9) for the fluorescence decay of excited donor chromophores ($I_D(t)$) in the presence of acceptors under conditions where the donor/acceptor concentrations obey cylindrical symmetry but can otherwise be arbitrary. The method enables one to evaluate $I_D(t)$ from a knowledge of the donor and acceptor concentration profiles, even when the translational invariance requirements of the Klafter−Blumen methodology are not satisfied. When the simplifying conditions are satisfied, our equations reduce to published results.

We also explored the possibility of using fluorescence decay measurements to distinguish spherical and cylindrical objects with the same surface-to-volume ratio in samples labeled with energy donor inside and acceptor dyes at the surface. We simulated a 7.5-nm-radius sphere and a 5-nm-radius cylinder (with donors inside and acceptors at the surface) and analyzed the corresponding fluorescence decay curves using the model for spherical structures. Although for the sphere we recovered a radius of $R_S = 7.5 \pm 0.5$ nm, for the cylindrical geometry the equivalent spherical radius obtained, $R_S = 6.7 \pm 0.5$ nm, is about 35% higher than the real cylinder radius ($R_C = 5$ nm). The very low detection limit of fluorescence measurements and the high sensitivity of DET to the geometry of the dyes' distribution open up interesting possibilities regarding structure identification in nanomaterials and surfaces.[46]

Acknowledgment. We thank Professor M. D. Whitmore and Mr. J. D. Vavasour for information and useful discussions on the morphology of block copolymers of hexagonally stacked cylinders, to be further considered in the companion paper[28] to this publication. J.P.S.F. acknowledges financial support from FCT and FEDER (project POCTI/QUI/47885/2002). The Toronto authors thank NSERC Canada and the Province of Ontario through its ORDCF program for their financial support.

Appendix

As mentioned in the Model section of this article, we will address here the equivalence of the BKZ model, eq 14 (for donors randomly distributed on the surface and acceptors inside a cylinder of radius R and infinite length, Figure 2c), and our approach for very short decay times after excitation. As we have also mentioned, by "very short" we mean times where in the expansion of the exponential functions, we may neglect terms of power 2 and higher, resulting in the local survival probability expressions

$$-\ln[\phi(t)] = \frac{6C_A^0\kappa^2R_0^6t}{\tau_D}\int_0^{2R} dr \int_0^{\infty} dz\, r\cos^{-1}\left(\frac{r}{2R}\right)\left[\frac{1}{(z^2+r^2)^3}\right] \quad \text{(A1)}$$

for the BKZ model and

$$-\ln[\phi(t,\vec{r}_D)] = \frac{6C_A^0\kappa^2R_0^6t}{\tau_D}\left[\int_{R_e}^{\infty} dz_A \int_0^R R_A\, dR_A \int_0^{\pi} \times \frac{1}{(R^2+R_A^2+z_A^2-2RR_A\cos\theta_A)^3}\, d\theta_A + \int_0^{R_e} dz_A \int_0^{R-R_e} R_A\, dR_A \int_0^{\pi} \times \frac{1}{(R^2+R_A^2+z_A^2-2RR_A\cos\theta_A)^3}\, d\theta_A + \int_0^{R_e} dz_A \int_{R-R_e}^{R} R_A\, dR_A \int_{\beta}^{\pi} \times \frac{1}{(R^2+R_A^2+z_A^2-2RR_A\cos\theta_A)^3}\, d\theta_A\right] \quad \text{(A2)}$$

with $\beta = \cos^{-1}[(R^2 + R_A^2 - R_e^2)/(2RR_A)]$ for our model.

It appears that Blumen, Klafter, and Zumofen were able to obtain an analytic expression for eq A1;[22] they have not published details of their derivation, and in any event, it will be instructive to compare numerical integration results of eqs A1 and A2. To do so, we have assumed a cylinder of 5 nm

radius. The latter assumption was motivated by attempting to consider an R/R_0 value of approximately 2. (We frequently work with phenanthrene and anthracene as a donor−acceptor pair, where R_0 has been determined to be 2.3 nm.[37]) Levitz, Drake, and Klafter reported interesting crossover effects for similar circumstances.[21] To investigate the applicability of our model, it was also desirable to introduce into the BKZ formulation the same restriction concerning minimum donor−acceptor separations as in eqs 7 and 8 (i.e., an exclusion cylinder of radius R_e and height $2R_e$). We assumed that $R_e = 0.5$ nm, as before.

The BKZ model, modified for 0.5-nm donor−acceptor encounter distance, now requires the computation of

$$\int_{0.5}^{10} \mathrm{d}r \int_0^{\infty} \mathrm{d}z \frac{r \cos^{-1}(r/10)}{(z^2+r^2)^3} + \int_0^{0.5} \mathrm{d}r \int_{0.5}^{\infty} \mathrm{d}z \frac{r \cos^{-1}(r/10)}{(z^2+r^2)^3} \quad \text{(A3)}$$

The first double integral of A3 can actually be evaluated analytically, employing the integration equations[47]

$$\int \frac{\mathrm{d}x}{(a^2+x^2)^3} = \frac{x}{4a^2(a^2+x^2)^2} + \frac{3x}{8a^4(a^2+x^2)} + \frac{3}{8a^5}\tan^{-1}\frac{x}{a} + C \quad \text{(A4)}$$

and

$$\int \frac{\mathrm{d}x}{x^4}\cos^{-1}\frac{x}{a} = -\frac{1}{3x^3}\cos^{-1}\frac{x}{a} + \frac{(a^2-x^2)^{1/2}}{6a^2x^2} + \frac{1}{6a^3}\ln\left|\frac{a+(a^2-x^2)^{1/2}}{x}\right| + C \quad \text{(A5)}$$

This approach cannot be employed for the second improper integral component of A3 because the inner integral diverges as r tends to zero. However, numerical double integrations[40] to finite values of z and then extrapolation to $z \rightarrow \infty$ gave very satisfactory results, as evidenced by obtaining the same result when the order of the integrations was reversed. The value we obtained for the sum of the integrals in eq A3 was 2.9374085. (We specified a precision of 5×10^{-8} for the numerical integrations.)

Our model (again, with a 0.5-nm donor−acceptor encounter distance) leads to the sum of the volume integrals A6 to A8 (instead of A3):

$$\iiint_{\{(\Theta_A,R_A,z_A)\}=[0,\pi]\times[0,5]\times[0.5,\infty)} \times \frac{R_A}{(25+R_A^2+z_A^2-10R_A\cos\theta_A)^3}\,\mathrm{d}V \quad \text{(A6)}$$

$$\iiint_{\{(\Theta_A,R_A,z_A)\}=[0,\pi]\times[0,4.5]\times[0,0.5]} \times \frac{R_A}{(25+R_A^2+z_A^2-10R_A\cos\theta_A)^3}\,\mathrm{d}V \quad \text{(A7)}$$

$$\iiint_{\{(\Theta_A,R_A,z_A)\}=[\beta,\pi]\times[4.5,5]\times[0,0.5]} \times \frac{R_A}{(25+R_A^2+z_A^2-10R_A\cos\theta_A)^3}\,\mathrm{d}V \quad \text{(A8)}$$

where $\beta = \cos^{-1}(24.75 + R_A^2)/10R_A$.

Regarding A6, we note that $25 + R_A^2 - 10R_A\cos\theta_A \geq (5 - R_A)^2 \geq 0$, ensuring uniform convergence as $z_A \rightarrow \infty$. Thus, the volume integral A6 may be evaluated as[48]

$$\iint_{\{(R_A,z_A)\}=[0,5]\times[0.5,\infty)} R_A\,\mathrm{d}A \int_0^{\pi} \times \frac{\mathrm{d}\theta_A}{(25+R_A^2+z_A^2-10R_A\cos\theta_A)^3} = \quad \text{(A9)}$$

$$\pi \iint_{\{(R_A,z_A)\}=[0,5]\times[0.5,\infty)} R_A \times \frac{(25+R_A^2+z_A^2)^2+50R_A^2}{[(25+R_A^2+z_A^2)^2-100R_A^2]^{5/2}}\,\mathrm{d}A$$

(The differential dA denotes area integration.)

The double-integration software, after extrapolation to $z_A \rightarrow \infty$, yielded 1.0077125 for A6. In a similar manner (without extrapolation), we obtained 0.7469086 for A7.

For A8, we note that $25 + R_A^2 - 10R_A\cos\theta_A \geq 0.25$ over the integration range so that eq A4 may be employed to integrate over z_A, followed by numerical double integration over θ_A and R_A. This gave 1.1827874 for A8. To the precision specified, our model has thus yielded *exactly* the same result as the corresponding Blumen−Klafter−Zumofen equation, A3.

References and Notes

(1) Krausch, G.; Magerle, R. *Adv. Mater.* **2002**, *14*, 1579.
(2) Fredrickson, G. H.; Helfand, E. *J. Chem. Phys.* **1987**, *87*, 697.
(3) Bates, F. S.; Fredrickson, G. H. *Annu. Rev. Phys. Chem.* **1990**, *41*, 525.
(4) Stamm, M.; Schubert, D. W. *Annu. Rev. Mater. Sci.* **1995**, *25*, 325.
(5) Torikai, N.; Noda, I.; Karim, A.; Satija, S. K.; Han, C.; Matsushita, Y.; Kawakatsu, T. *Macromolecules* **1997**, *30*, 2907.
(6) Sidorenko, A.; Tokarev, I.; Minko, S.; Stamm, M. *J. Am. Chem. Soc.* **2003**, *125*, 12211.
(7) Park, M.; Harrison, C.; Chaikin, P. M.; Register, R. A.; Adamson, D. H. *Science* **1997**, *276* 1401.
(8) Turn-Albrecht, T.; Steiner, R.; DeRouchey, J.; Stafford, C. M.; Huang, E.; Bal, M.; Tuominen, M.; Hawker, C. J.; Russell, T. P. *Adv. Mater.* **2000**, *12*, 787.
(9) Liu, G.; Li, Z.; Yan, X. *Polymer* **2003**, *44*, 7721.
(10) Wang, X.-S.; Arsenault, A.; Ozin, G. A.; Winnik, M. A.; Manners, I. *J. Am. Chem. Soc.* **2003**, *125*, 12686.
(11) Templin, M.; Franck, A.; Du Chesne, A.; Leist, H.; Zhang, Y.; Ulrich, R.; Schadler, V.; Wiesner, U. *Science* **1997**, *278*, 1795.
(12) Harper, T.; Román Vas, C.; Holister P. *Chem. Eng. Prog.* **2003**, *99* (11), 33S.
(13) Yekta, A.; Winnik, M. A. In *Solvents and Self-Organization of Polymers;* Webber, S. E., Munk, P., Tuzar, Z., Eds.; Kluwer: Dordrecht, The Netherlands, 1996; pp 433−455.
(14) Webber, S. E. *Macromol. Symp.* **1999**, *143*, 359.
(15) Klafter, J.; Blumen, A.; Drake, J. M. In *Molecular Dynamics in Restricted Geometries*; Klafter, J.; Drake, J. M., Eds.; John Wiley and Sons: New York, 1989; pp 1−22. Levitz, P.; Drake, J. M.; Klafter, J. In *Molecular Dynamics in Restricted Geometries*; Klafter, J.; Drake, J. M., Eds.; John Wiley and Sons: New York, 1989; pp 165−195.
(16) Pekcan, Ö.; Winnik, M. A. *Chem. Phys.* **1990**, *146*, 283.
(17) Tcherkasskaya, O.; Ni, S.; Winnik, M. A. *Macromolecules* **1996**, *29*, 4241.
(18) O'Connor, D. V.; Phillips, D. *Time-Correlated Single Photon Counting*; Academic Press: London, 1984.
(19) Förster, Th. *Ann. Phys.* **1948**, *2*, 55. Förster, Th. *Z. Naturforsch., A* **1949**, *4*, 321.
(20) Gochanour, C. R.; Fayer, M. D. *J. Chem. Phys.* **1979**, *70*, 4254. Gochanour, C. R.; Andersen, H. C.; Fayer, M. D. *J. Phys. Chem.* **1981**, *85*, 1989. Loring, R. F.; Andersen, H. C.; Fayer, M. D. *J. Chem. Phys.* **1982**, *76*, 2015. Miller, R. J. D.; Pierre, M.; Fayer, M. D. *J. Chem. Phys.* **1983**, *78*, 5138.
(21) Levitz, P.; Drake, J. M.; Klafter, J. *Chem. Phys. Lett.* **1988**, *148*, 557.

(22) Blumen, A.; Klafter, J.; Zumofen, G. *J. Chem. Phys.* **1986**, 84, 1397.

(23) Berberan-Santos, M. N.; Prieto, M. *J. Chem. Soc., Faraday Trans. 2* **1987**, *83*, 1391.

(24) Farinha, J. P. S.; Martinho, J. M. G.; Yekta, A.; Winnik, M. A. *Macromolecules* **1995**, *28*, 6084.

(25) Yekta, A.; Duhamel, J.; Winnik, M. A. *Chem. Phys. Lett.* **1995**, *235*, 119.

(26) Farinha, J. P. S.; Martinho, J. M. G.; Kawaguchi, S.; Yekta, A.; Winnik, M. A. *J. Phys. Chem.* **1996**, *100*, 12552.

(27) Yekta, A.; Winnik, M. A.; Farinha, J. P. S.; Martinho, J. M. G. *J. Phys. Chem. A* **1997**, *101*, 1787.

(28) Spiro, J. G.; Farinha, J. P. S.; Winnik, M. A.; Vavasour, J. D.; Whitmore, M. D., to be submitted for publication.

(29) Vavasour, J. D.; Whitmore, M. D. *Macromolecules* **1992**, *25*, 5477.

(30) Arnold, M.; Hofmann, S.; Weidisch, R.; Michler, G. H.; Neubauer, A.; Poser, S. *Macromol. Chem. Phys.* **1998**, *199*, 31.

(31) Weidisch, R.; Michler, G. H.; Fischer, H.; Arnold, M.; Hofmann, S.; Stamm, M. *Polymer* **1999**, *40*, 1191.

(32) Lamarche, F.; Leroy, C. *Comput. Phys. Commun.* **1990**, *59*, 359.

(33) Baumann, J.; Fayer, M. D. *J. Chem. Phys.* **1986**, *85*, 4087.

(34) Martinho, J. M. G.; Farinha, J. P.; Berberan-Santos, M. N.; Duhamel, J.; Winnik, M. A. *J. Chem. Phys.* **1992**, *96*, 8143.

(35) Buck, R. C.; Buck, E. F. *Advanced Calculus*, 2nd ed.; McGraw-Hill: New York, 1965; pp 204−212.

(36) Farinha, J. P. S.; Schillén, K.; Winnik, M. A. *J. Phys. Chem. B* **1999**, *103*, 2487.

(37) Wang, Y.; Zhao, C.-L.; Winnik, M. A. *J. Chem. Phys.* **1991**, *95*, 2143.

(38) Lakowicz, J. R. *Principles of Fluorescence Spectroscopy*; Plenum: New York, 1983; pp 271−276.

(39) See, for example, Marsden, J. E.; Tromba, A. J. *Vector Calculus*, 3rd ed.; W. H. Freeman and Co.: New York, 1988; pp 440−454.

(40) *NAG Fortran Library, Mark 15*; The Numerical Algorithms Group Limited: Oxford, U.K., 1991.

(41) Gill, P. E.; Miller, G. F. *Comput. J.* **1972**, *15*, 80.

(42) Hager, W. W. *Applied Numerical Linear Algebra*; Prentice Hall: Englewood Cliffs, NJ, 1988; pp 30−33.

(43) James, D. R.; Demmer, D. R. M.; Verrall, R. E.; Steer, R. P. *Rev. Sci. Instrum.* **1983**, *54*, 1121.

(44) Farinha, J. P. S.; Martinho, J. M. G.; Pogliani, L. *J. Math. Chem.* **1997**, *21*, 131.

(45) Yekta, A.; Spiro, J. G.; Winnik, M. A. *J. Phys. Chem. B* **1998**, *102*, 7960.

(46) McArthur, E. A.; Ye, T.; Cross, J. P.; Petoud, S.; Borguet, E. *J. Am. Chem. Soc.* **2004**, *126*, 2260.

(47) Dwight, H. B. *Tables of Integrals and Other Mathematical Data*, 4th ed.; Macmillan: New York, 1961.

(48) Gradshteyn, I. S.; Ryzhik, I. M. *Table of Integrals, Series, and Products*, 5th ed.;Academic Press: Boston, 1994.

(49) The discussion in this section deals with cylinders of "infinite" length. What we mean by infinite in the DET context is that the fraction of donors near the edges is so small (say, less than 1%) as to make a negligible contribution to the $I_D(t)$ signal.[13] Obviously, this requires the nanocylinders to have a high aspect ratio.